Biosensors and Bioelectronics 26 (2011) 4032–4039

Contents lists available at ScienceDirect

Biosensors and Bioelectronics

journal homepage: www.elsevier.com/locate/bios

A new impedimetric biosensor utilizing VEGF receptor-1 (Flt-1): Early diagnosis of vascular endothelial growth factor in breast cancer

Mustafa Kemal Sezgintürk*

Namık Kemal University, Faculty of Science, Chemistry Department, Biochemistry Division, Tekirdağ, Turkey

ARTICLE INFO

Article history:
Received 16 December 2010
Received in revised form 22 March 2011
Accepted 27 March 2011
Available online 2 April 2011

Keywords:
VEGF-R1
VEGF
Breast cancer
Electrochemical impedance spectroscopy
Biosensor

ABSTRACT

A new impedimetric biosensor, based on the use of vascular endothelial growth factor receptor-1 (VEGF-R1), was developed for the determination of vascular endothelial growth factor (VEGF). VEGF-R1 was immobilized through covalent coupling with 3-mercaptopropionic acid which formed a self-assembled monolayer on gold electrodes. Cyclic voltammetry (CV) and electrochemical impedance spectroscopy techniques were employed to characterize the immobilization process and to detect VEGF. To successfully construct the biosensor current, experimental parameters were optimized. Kramers–Kronig Transform was performed on the experimental impedance data. The obtained results provided a linear response range from 10 to 70 pg/mL human VEGF. The applicability of the developed biosensor in the determination of VEGF in a spiked artificial human serum sample was experienced, yielding average recovery of 101%, in that order, with an average relative deviation value less than 5%.

1. Introduction

Breast cancer is one of the most frequently diagnosed cancers among women in the world. Due to the aggressive behaviour of some specific types and the possibility of an early diagnosis, breast cancer has been constantly studied in relation to diagnostic and treatment methods (Dhingra and Hortobagyi, 1996; Levenson, 2007; Oldenburg et al., 2007). Although current morphological features such as tumour size, histological type, cellular and nuclear characteristics, mitotic index, necrosis, vascular invasion, hormonal receptors and axillary tumour lymph node status are routinely used they are not sufficient for diagnosis of breast cancer (Sjostrom et al., 2000; Laguens et al., 2010). Fortunately, developments in molecular biology have led to the discovery of novel biomarkers that can show the stage of the disease. These biomarkers are extremely valuable tools for establishing whether the patient has a good or bad prognosis (Kulasingam and Diamandis, 2007; Sawyers, 2008). DNAs, mRNAs, cell surface receptors, transcription factors, and secreted proteins can behave as potential cancer biomarkers (Wang et al., 2009; Boffetta, 2010). In connection with this, VEGF is an important regulator of angiogenesis and vascular permeability, and is considered the most powerful mitogen for endothelial cells. It is secreted by tumour cells and by stromal monocytes and macrophages, responding to stimuli such as hypoxia or cytokines (IL 1, 3, 6 and 10). In breast cancer, VEGF is used as a marker of unfavourable prognosis since it is associated with recurrence. Because angiogenesis is essential for growth and tumour progression, the use of its inhibitors is becoming of interest as a co-adjuvant of other therapies. It has been observed that patients with metastasis have higher levels of serum VEGF and could benefit from anti-VEGF treatment (Sidoni et al., 2001; Adams et al., 2000; Rampaul et al., 2005; Lo et al., 2005; Rochefort et al., 2000; Gonzalez Campora et al., 2000).

The aim of the study is to establish the design of an electrochemical biosensor system based on electrochemical impedance spectroscopy which will enable fast, sensitive, and practical determination of the breast cancer biomarker, VEGF, which comes into being often in the field of clinics and threatens people, especially women. Previously, a number of determination systems for VEGF have been reported. Lee et al. (2009) reported on a label-free and electrical method of the detection of VEGF using anti-VEGF aptamer-modified Si nanowire field-effect transistors. Prabhulkar et al. (2009) also reported a biosensor based on ferrocene monocarboxylic acid labelled anti-VEGF which was covalently immobilized on the microelectrode surface. The biosensor allowed VEGF analysis with a limit of detection of about 38 pg/mL.

Recently, EIS has become an efficient method used for many chemical and physical processes. EIS presents analytic solutions for many processes. Besides these, identification of membranes, and biosensor characterization and fabrication could also be effectively monitored by EIS. Conversely enzyme–substrate interactions, after antigen–antibody, receptor–ligand, or DNA–DNA interactions which have no catalytic reaction could be succes-

* Tel.: +90 282 293 3866.
E-mail addresses: msezginturk@hotmail.com, msezginturk@nku.edu.tr

0956-5663/$ – see front matter © 2011 Elsevier B.V. All rights reserved.
doi:10.1016/j.bios.2011.03.025

sively monitored by EIS (Bott, 2001; Katz and Willner, 2003; Guan et al., 2004). In the current study, human vascular endothelial growth factor receptor-1 (VEGF-R1, Flt-1) was used as a biorecognition element for the first time. Recombinant human VEGF-R1 is a disulfide-linked dimeric protein with two 905 amino acid residue polypeptides. It has a predicted monomeric molecular mass of 100 kDa (Shibuya et al., 1990; Kendall and Thomas, 1993; Neufeld et al., 1999). The recombinant soluble VEGF-R1 binds VEGF with high affinity (He et al., 1999; Olofsson et al., 1998; Conn et al., 1990). In the study, it was planned to develop a biosensor based on VEGF-R1 and electrochemical impedance spectroscopy to analyze VEGF, which was a potent biomarker of breast cancer. VEGF-R1 was covalently immobilized on gold electrodes by self-assembled monolayers. On the basis of cyclic voltammetry and electrochemical impedance investigations, we demonstrated that immobilization steps could be achieved. For analyzing EIS data it fitted to an equivalent circuit model. Certain important parameters, such as the DC potential applied to the system, were optimized for obtaining the best results. Finally, artificial serum samples spiked with VEGF were analyzed by the biosensor.

2. Experimental

2.1. Materials and instrumentation

All reagents were of analytical grade unless stated otherwise, and were purchased from Sigma–Aldrich (St. Louis, MO, USA). VEGF receptor-1 (Flt-1)/Fc Chimera (human) and Vascular endothelial growth factor (human) were purchased from Sigma–Aldrich (St. Louis, MO, USA). The content of the vials of VEGF was reconstituted in ultra pure water. VEGF solutions were prepared in two concentrations, which were 0.02 mg/mL and 0.1 mg/mL. Further dilutions were made using sterile phosphate buffer (pH 7, 0.01 M). The vials of VEGF-R1 were reconstituted using sterile phosphate buffer (pH 7 and 0.01 M) containing 0.1% bovine serum albumin. The final concentration of VEGF-R1 solution was 0.1 mg/mL. VEGF-R1 and VEGF portions were prepared at certain concentrations and were stored at −20 °C until use. Artificial serum solution was prepared using 4.5 mM KCl, 5 mM $CaCl_2$, 1.6 mM $MgCl_2$, 4.7 mM D(+)-glucose, 2.5 mM urea, 0.1% human serum albumin, and 145 mM NaCl. A three-electrode system, consisting of a gold working electrode (with a surface area of 2.01 mm^2), an Ag/AgCl (saturated KCl) reference electrode and a Pt counter electrode, was accommodated in a 10-mL electrochemical cell (all the electrodes were obtained from iBAS, Warwickshire, UK). Electrochemical experiments were performed using a Gamry Potentiostate/Galvanostate, Reference 600 (Gamry Instruments, Warminster, USA) interfaced with a PC *via* a EChem Analyst containing physical electrochemistry, pulse voltammetry, and electrochemical impedance spectroscopy software (Gamry Instruments, Warminster, USA). In all electrochemical experiments a faraday cage (from iBAS, Warwickshire, UK) was used to block out external static electric fields.

2.2. Preparation of the self-assembled monolayer of 3-mercaptopropionic acid

Prior to use, the surfaces of the Au electrodes were polished with 0.05 μm Al_2O_3 powder and then washed ultrasonically in deionized water for 5 min to remove alumina particles. Then the electrodes were immersed in Piranha (H_2O_2/H_2SO_4, 30/70, v/v) solution for 3 min. Following that the electrodes were washed with ultra pure water by immersion into water twenty times. For the next step, the surfaces of the electrodes were dried by a pure argon stream. This polishing and cleaning procedure was repeated before every electrode preparation step. The clean gold electrodes were immediately immersed into 3-mercaptopropionic acid solution (0.1 M, in pure ethanol) for 18 h. After this period, they were rinsed with ethanol and gently dried with an argon stream.

2.3. Covalent immobilization of VEGF-R1 on SAM of 3-MPA

For VEGF-R1 immobilization, 1-ethyl-3-(3-dimehylaminopropyl)carbodiimide (EDC) was used as a heterobifunctional crosslinker. N-hydroxysuccinimide (NHS) was used in conjunction with the crosslinker EDC. The gold electrodes were dipped in a glass bottle containing EDC/NHS solution (0.04 mM EDC, 0.01 mM NHS) for an hour in a dark ambient. Later, the gold electrodes were washed with ultra pure water gently, and were then dried by a pure argon stream again. In the last step, 5 μL of VEGF-R1 portion was applied to the active electrode surface by a pipette. The electrode was allowed to incubate for an hour in a moisture medium. Finally the electrode was immersed in ultra pure water to remove physically adsorbed VEGF-R1 molecules. The bare gold electrodes and the modified electrodes were denoted as Au, Au/3-MPA, Au/3-MPA/EDC-NHS, and Au/3-MPA/EDC-NHS/VEGFR1.

2.4. Electrochemical measurements

Cyclic voltammetry was used to characterize SAM formation on the bare gold electrodes, and the modified electrodes with different layers. The potential was varied between −100 and 500 mV (step size: 20 mV, scan rate: 50 mV/s) in the presence of a 5 mM $K_3[Fe(CN)_6]/K_4[Fe(CN)_6]$ (1:1) solution which served as a redox probe containing 0.1 M KCl. For electrochemical impedance studies, an alternating wave of 10 mV amplitude was applied to the electrode over the formal potential of the redox couple (0 V). The redox couple used for the impedance studies was the same as cyclic voltammetry. Impedance spectra were collected in the frequency range between 10,000 and 0.05 Hz.

2.5. Measurement procedure

After each of the VEGF-R1 biosensors was assembled, the biosensor surface was used to interact with VEGF solution. The standard solution of VEGF was injected onto the biosensor surface by a micro-pipette. The concentrations of standard VEGF solutions were 10, 20, 30, 40, 50, 60, and 70 pg/mL, respectively. For each time measurement, the injection volume was 5 μL. The response value was read after 1 h of incubation in a moisture medium. After the incubation period, the biosensor was gently immersed into the ultra pure water ten times to remove physically adsorbed VEGF molecules. Finally, the biosensor was again put into the cell containing $Fe(CN)_6^{4-/3-}$ redox probe solution, and the electrochemical measurements were taken as described in the previous section. The difference in charge transfer resistance between the biosensor unbounded and bounded VEGF was used for preparing of VEGF calibration curves.

3. Results and discussion

3.1. Cyclic voltammetry and electrochemical impedance spectroscopy of the biosensor in the presence of a redox probe

The changes of the modified gold electrodes with SAM and VEGF-R1 were investigated using CV and EIS. In the experiments, the redox couple $Fe(CN)_6^{3-/4-}$ was preferred for use as an electrochemical probe because $Fe(CN)_6^{3-/4-}$ showed a good integrity of SAM on gold, for example in regard to factors such as the pinhole degree or defect structure, insulating properties, and the density

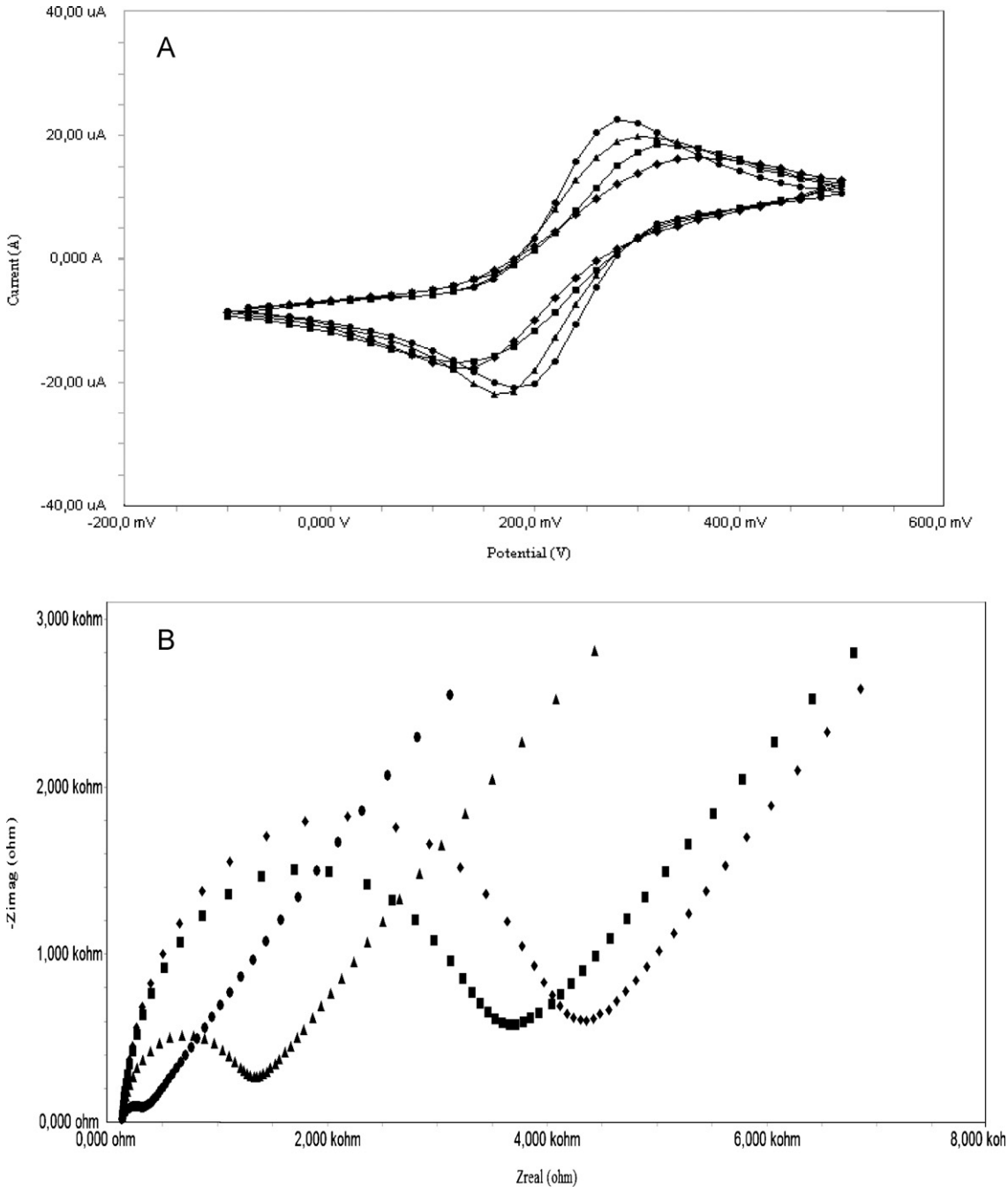

Fig. 1. (A) Cyclic voltammograms of VEGF-R1immobilization steps (-●-●-: bare gold electrode, -♦-♦-: Au/3-MPA, -▲-▲-: Au/3-MPA/EDC-NHS, -■-■-: Au/3-MPA/EDC-NHS/VEGF-R1). (B) Electrochemical impedance spectra of VEGF-R1 immobilization steps (-●-●-: bare gold electrode, -♦-♦-: Au/3-MPA, -▲-▲-: Au/3-MPA/EDC-NHS, -■-■-: Au/3-MPA/EDC-NHS/VEGF-R1).

of the adsorbed layer (Qingwen et al., 2001; Pei et al., 2001; Ding et al., 2005). First of all, it must be stressed that the cleaning of the gold electrode was a step of critical importance for self-assembled monolayer formation, and this must be accomplished systematically. In Fig. 1A, a well-defined characteristic voltammogram of the redox couple can be observed on the bare gold electrode. It was obvious that the anodic and cathodic current at a gold electrode decreased after self-assembly of 3-mercaptopropionic acid on the gold electrode surface. This was caused by the blocking effect of 3-MPA SAMs. After the next step, the EDC/NHS activation of terminal –COOH groups of 3-MPA SAMs, the peak current increased considerably compared to that obtained at a Au/3-MPA. The EDC/NHS reaction included formation of an intermediate active ester which was the product of condensation of terminal –COOH of 3-MPA and N-hydroxysuccinimide. This intermediate product exhibited excellent electrochemical activity. Moreover, although the carboxyl groups of 3-MPA could be reacted directly with amines using EDC, the reaction was much more efficient with NHS because a stable intermediate was created. In the activation step, it was possible to make electrochemical measurements just by this relatively stable intermediate product.

The peak current decreased after VEGF-R1 was immobilized onto the Au/3-MPA/EDC-NHS. The decrease was attributed to the fact that VEGF-R1 insulated the Au/3-MPA/EDC-NHS surface and hindered the transfer of electrons towards the electrode surface.

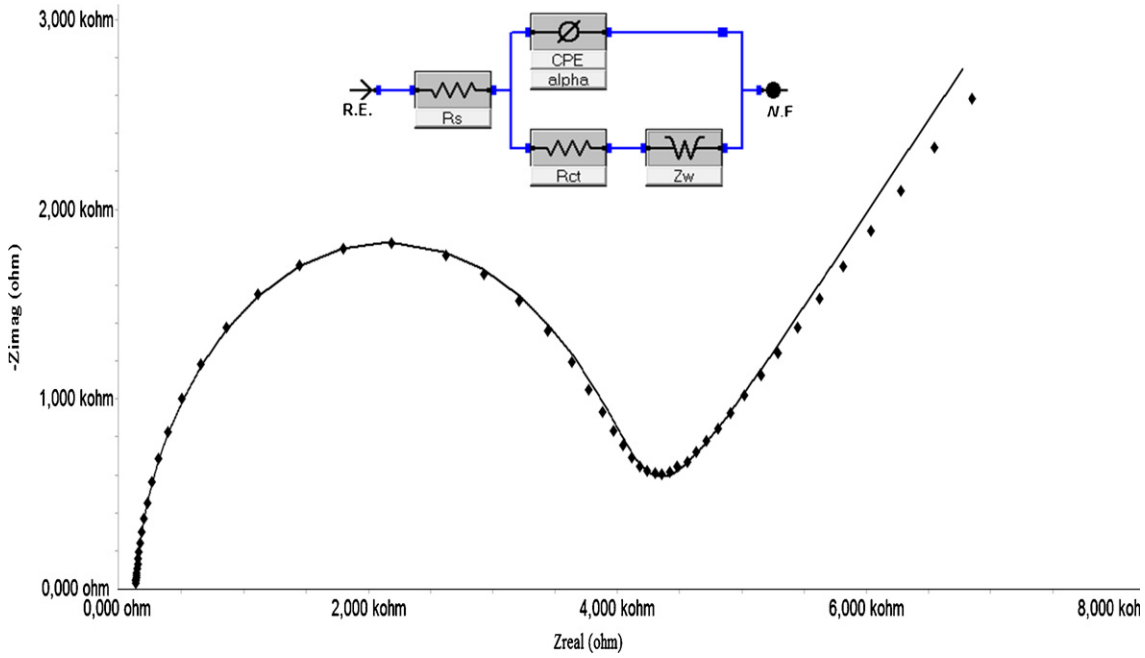

Fig. 2. Equivalent circuit model applied to fit the impedance measurements. (Circles: experimental spectrum, line: fitted spectrum. Rs, the ohmic resistance of the electrolyte solution; CPE, associated with the double layer capacitance; R_{ct}, the electron transfer resistance and Zw, the Warburg impedance.)

As mentioned earlier, EIS is a very useful technique for investigating the surface characteristics of a material. Fig. 1B shows the impedance responses of a redox probe on bare Au, Au/3-MPA, Au/3-MPA/EDC-NHS, and Au/3-MPA/EDC-NHS/VEGF-R1. The R_{ct} values were 204.3, 3294, 1121, and 3920 Ω, respectively. In Nyquist plots, the semicircle diameter at higher frequencies corresponds to the electron-transfer resistance (R_{ct}) and the linear part at lower frequencies corresponds to the diffusion process (Warburg impedance). Moreover the larger the semicircle diameter in the complex plane was, the larger the value of R_{ct}. The diameter of the semicircle also exhibited the blocking behaviour of the modified electrode after each modification step. As can be seen from Fig. 2, the impedance data were successively fitted with commercial software called Gamry Echem Analyst. The equivalent circuit model was used to interpret impedance data. An overlay of the fitted spectrum and experimental spectrum obtained for Au/3-MPA/EDC-NHS/VEGF-R1 can be seen in Fig. 2. These curves indicated good agreement between the circuit model and the system, especially in the higher frequencies.

From Fig. 1B, the smaller semicircle diameter was obtained with an Au electrode. This indicated the faster electron transfer of the redox probe on the bare gold electrode surface. The semicircle diameter, R_{ct}, increased with self-assembly of 3-MPA on gold electrode. The increase in R_{ct} was associated with the blocking

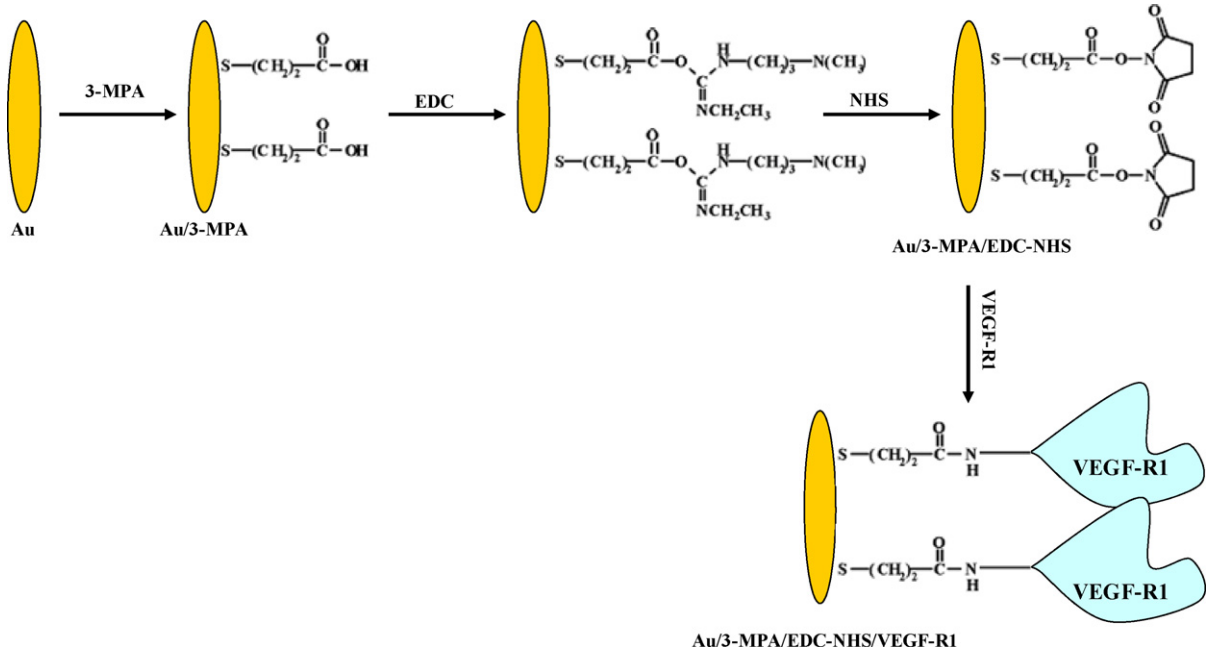

Fig. 3. Schematic representation of VEGF-R1 immobilization process on gold electrodes.

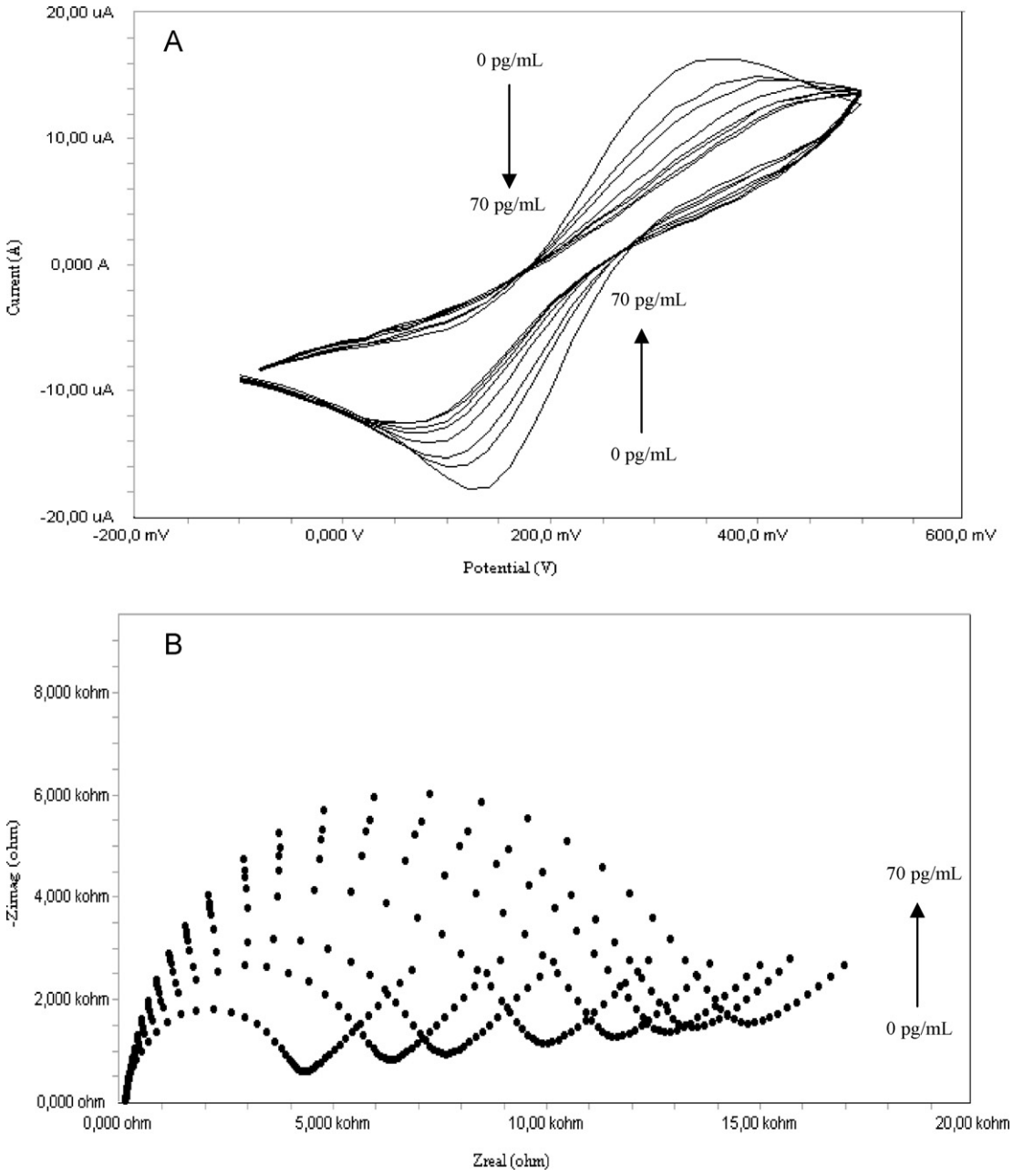

Fig. 4. Cyclic voltammograms (A) and impedance spectra (B) for vascular endothelial growth factor concentrations.

behaviour of the self-assembled layer of 3-MPA on the electrode surface for the $Fe(CN)_6^{3-/4-}$ redox probe. Beside this blocking effect, terminal –COOH groups on the electrode surface presumably formed a surface which was negatively charged. Such a negatively charged surface showed electrostatic repulsive effects between the redox probe anion and $–COO^-$ groups. This effect contributed to the increase of the semicircle diameter. A decrease in R_{ct} value compared with that of Au/3-MPA electrode indicated the activation of terminal –COOH and formation of an active intermediate product. The result showed excellent agreement between cyclic voltammetry and electrochemical impedance spectroscopy studies. A considerable increase in R_{ct} after the Au/3-MPA/EDC-NHS was incubated with VEGF-R1 resulted from the successful immobilization of VEGF-R1 on the electrode surface. It can be concluded that there was a good linear relationship between semicircle diameters and electrode layers, which indicates successively construction of the biosensor. A schematic representation is given in Fig. 3.

3.2. Optimization experiments of VEGF-R1 biosensor

Firstly, the relationship between DC-potential and Nyquist plots was optimized. The results revealed that the effect of DC-potential applied to the system on Nyquist plots was very determinative. This was especially obvious when a DC-potential higher than 40 mV was applied to the system. The higher DC potentials drove the system far from equilibrium. A considerable current (about 2 μA) was formed by applying the potentials of 120 and 180 mV, and this current caused a change in the system. Of course, the impedance spectra diverged from their ideal forms unfavourable. Nyquist diagrams concerning different DC-potentials are given in Supplemental information in Fig. 1. Moreover, such a high current should also alter the ratio of concentrations of substances on the electrode surface. The Kramers–Kronig Transform was also performed on the experimental data. The results revealed the deviations on Nyquist plots at the lower frequencies. Moreover,

the electrochemical impedance spectra obtained by applying the higher DC-potentials to the system, there was a deviation on the portion of Warburg impedance of Nyquist diagram. Although the diagram seemed to show a Warburg element at first sight, in fact this was not the case. Because the angle of ω was not 45°, the impedance spectrum did not overlap with the theoretical data. Because of that, in the impedance measurements a DC-potential of 0 V was applied to the system.

The experiments showed that the response of the biosensor would be influenced by the concentrations of EDC/NHS. To study the effect of EDC/NHS concentrations, a –COOH activation procedure was carried out by differing EDC/NHS (mM) concentrations such as 4/1, 0.4/0.1, 0.04/0.01, and 0.004/0.001. The impedance spectra related to these findings can be seen in Supplemental information in Fig. 2. The accuracy and proficiency of immobilization of VEGF-R1 was directly dependent on this concentration ratio. The higher concentrations of EDC/NHS caused the Nyquist plots with diverging from Kramers–Kronig Transforms. Moreover, the activation with concentrations higher than 0.04/0.01 EDC/NHS showed that the binding of VEGF-R1 to active ester form could not be observed with the help of the impedance spectra because they had a shape which did not allow analysis of VEGF impedimetrically. Moreover, when a concentration ratio of 0.004/0.001 mM was used, VEGF-R1 was not effectively immobilized because of the insufficient degree of activation of terminal –COOH groups. Overall, the activation process of terminal –COOH groups was achieved using 0.04 mM EDC and 0.01 mM NHS, in all experiments.

Another parameter was VEGF-R1 incubation time, which could be optimized. The experiment results showed that the immobilization performance of VEGF-R1 was very dependent on the incubation time. The cyclic voltammograms and impedance spectra belonging to these experiments can be seen in Supplemental information in Fig. 3. R_{ct} values for the incubation periods for 1, 2, 4, and 6 h were 6539, 6008, 3701, and 2949 Ω, respectively. The immobilization of VEGF-R1 increased the charge transfer resistance drastically. This result was expected because of the blocking behaviour of the VEGF-R1 layer on the electrode surface for the redox probe $[Fe(CN)_6]^{3-/4-}$, which was reflected in the impedance spectroscopy as an increase in the diameter of the semicircle at high frequencies. Despite the charge transfer resistances, R_{ct}, decreased considerably with the increase in incubation times. At the end of the 6th hour of the incubation period, VEGF-R1 solution on the electrode surface had completely evaporated spontaneously although the electrode was incubated in a moisture medium. A similar result was also obtained for 4 h incubation. Probably, the immobilization performance of VEGF-R1 was negatively affected due to take a long time for incubation. However, it seemed that incubation periods shorter than 4 h caused the solution of VEGF-R1 to evaporate partially. The highest R_{ct} value was obtained after an incubation period of 1 h. Finally, according to the results obtained, it was shown to be efficient to incubate VEGF-R1 for an hour.

Eventually, the incubation period for binding between VEGF-R1 and VEGF was optimized. For this purpose VEGF-R1/VEGF interaction was realized using different incubation periods such as 1, 2, 4, and 6 h. The R_{ct} values obtained by different incubation periods were 11,460, 9063, 6814, and 4733 Ω, respectively. Very similar results were obtained in the studies of optimization for VEGF incubation periods to the study of VEGF-R1. The cyclic voltammograms and the impedance spectra can be seen in Supplemental information in Fig. 4. The binding ratio of VEGF to VEGF-R1 was decreased with an increase in incubation periods. This was probably caused by a similar effect to that of VEGF-R1 incubation. Because of that, the most effective period for VEGF incubation was an hour long. If VEGF-R1 and VEGF incubation periods are evaluated in terms of total measurement duration, short periods for both incubation processes should be favourable.

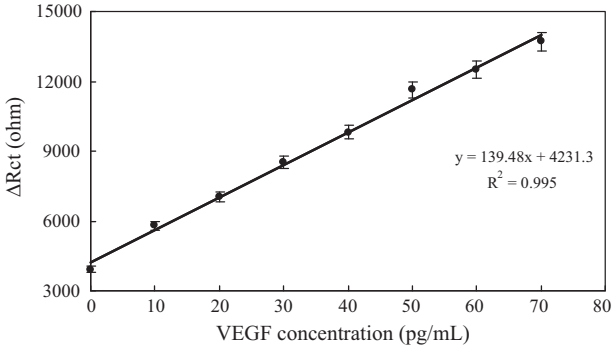

Fig. 5. VEGF calibration curve obtained at optimal working.

3.3. Analytical characteristics of VEGF-R1 biosensor

Fig. 4 shows the impedance spectra and the cyclic voltammograms obtained with the biosensor-based VEGF-R1. As can be seen in Fig. 4A, the R_{ct} value increased after VEGF was applied to the biosensor surface. This hindered the redox reaction of $[Fe(CN)_6]^{3-/4-}$, because an extra layer was formed on the surface. It is clear from the Nyquist plots that the low frequency ranges were particularly suitable for concentration-dependent impedance measurements.

The increment of VEGF concentration increased the charge transfer resistance, R_{ct}, achieving a linear range between 10 pg/mL and 70 pg/mL. A calibration graph for VEGF was prepared with the help of the differences in charge transfer resistances after VEGF binding. The calibration curve is given in Fig. 5.

The change of charge–transfer resistance differences was calculated by the following equation:

$$\Delta R_{ct} = R_{ct} - R_{ct}$$

where $R_{ct(VEGF\text{-}R1/VEGF)}$ is the value of the charge transfer resistance after VEGF-R1 was coupled to VEGF, while $R_{ct(VEGF\text{-}R1)}$ is the value of the charge transfer resistance when VEGF-R1 was immobilized on the electrode.

In this study, Kramers–Kronig Transform was one of the most important parameters analyzed. The Kramers–Kronig relations are integral equations that constrain the real and imaginary components of complex quantities for systems that satisfy conditions of linearity, causality, and stability (Kronig, 1926; Kramers, 1929; Orazem and Tribollet, 2008). In principle, the Kramers–Kronig relations can be used to determine whether the impedance spectrum of a given system has been influenced by bias errors caused, for example, by instrumental artefacts or time-dependent phenomena. This information is critical to the analysis and interpretation of electrochemical impedance spectroscopy data due to difficulties with their applications (Orazem and Tribollet, 2008). The Kramers–Kronig relations have been applied to electrochemical systems by direct integration of the equations, by experimental observation of stability and linearity, by regression of specific electrical circuit models, and by regression of generalized measurement models (Ehm et al., 2000; Huang et al., 2007). Direct integration of the Kramers–Kronig relations involves calculating one component of the impedance from the other, e.g., the real component of impedance from the measured imaginary component. The result is compared to the experimental values obtained (Orazem and Tribollet, 2008).

In the presented study, Kramers–Kronig Transforms were performed by the software called Gamry Echem Analyst (Ver. 5.61). The calculation was carried out following the method used by Boukamp (1995). Real experimental data was used to calculate the imaginary parts of a linear, stable, and causal circuit. Likewise, the imaginary portion of the experimental data was used to calculate the

Table 1
The results for Kramers-Kronig Transforms, Reproducibility, and the sample analysis.

Biosensor surfaces			Goodness of fit values
Kramers–Kronig transforms for different layers of the biosensor			
Bare Au			2.135
Au/3-MPA			3.824
Au/3-MPA/EDC-NHS			12.34
Au/3-MPA/EDC-NHS/VEGF-R1			3.294
Au/3-MPA/EDC-NHS/VEGF-R1-VEGF			1.001
Biosensor numbers	**R^2**	***y***	**Linear ranges (pg/mL)**
Reproducibility of the biosensor			
1	0.993	$136.4x + 4068$	0–70
2	0.993	$135.4x + 4159$	0–70
3	0.989	$133.2x + 4278$	0–70
4	0.991	$131.6x + 4502$	0–70
5	0.991	$134.5x + 4307$	0–70
6	0.989	$139.6x + 4019$	0–70

VEGF (pg/mL)

Added	Found by the biosensor	% recovery	% relative difference
VEGF detection in artificial serum samples			
20	21.1	105.5	5.5
40	40.6	101.5	1.5
60	57.6	96	4

real part of a linear, stable, and causal circuit. According to this calculation, a value named "goodness of fit" was obtained. In addition, a plot of the relative errors ($\Delta Z/Z$) for the real and imaginary parts of the experimental data was drawn. For the present new biosensor, for all steps including preparation of the biosensor and measurement, Kramers–Kronig Transforms were performed. The plots of the Kramers–Kronig Transforms are given in Supplemental information in Fig. 5. The goodness of fit values of different biosensor surfaces are also given in Table 1.

The Kramers–Kronig Transforms performed on the electrochemical impedance spectra related the biosensor revealed that the experimental data agreed with the data obtained by the transform. Nevertheless, it was very important that the impedance spectra were linear, stable, and causal circuit. Finally, it was also significant that the system was not influenced by unknown variables.

The charge transfer resistances of the biosensor were investigated when it was consecutively exposed to a 20 pg/mL VEGF standard solution ten times. The repeatability of the measurements was very good considering that the correlation coefficient on measurements was 1.94%, and average value and standard deviation were calculated as 20.12 pg/mL and ±0.39 pg/mL, respectively. The results showed that the biosensor exhibited a fairly desirable analytical feature of repeatability. The reproducibility of six identical biosensors was also examined. The linear detection ranges of three biosensors were the same as 10–70 pg/mL. The results are given in Table 1. The biosensor described here also provided excellent reproducibility. The results are again summarized in Table 1.

The stability of the biosensor was also examined over a 20-day period by performing measurements of 40 pg/mL of VEGF at the end of certain storage periods. For this purpose each biosensor was separately stored for between 1 and 20 days under dry conditions at 4 °C. These results are given in Supplemental information in Fig. 6. The results showed that there was no significant change in the response of impedance. This good stability increased the usefulness of the proposed biosensor. Besides developing the capability of the biosensor to specifically detect VEGF, the biggest challenge was to enable error-free measurement. For the evaluation of the specificity of the proposed biosensor, certain interferences such as hemoglobin, IgM, IgA, IgG, c-ERB, albumin, insulin, glucose, Asp, Glu, Lys, and His which could exist in human blood were examined. The impedance spectrums related to these experiments are given in Supplemental information in Fig. 7. From the results, these proteins and substances did not interfere with the biosensor. Also, in the charge transfer values related to the substances tested there were no meaningful changes.

To illustrate the feasibility of the biosensor in practical analysis, the artificial serum samples were prepared by the addition of VEGF standard solutions. These artificial serum samples were analyzed using the proposed impedimetric biosensor based on VEGF-R1. As shown in Table 1, the data were in good agreement between the added amount and the detected amount.

4. Conclusion

In this work, an impedimetric biosensor utilizing vascular endothelial growth factor receptor-1, VEGF-R1, was successfully developed. In the literature, VEGF-R1 was used for the first time for construction of an impedimetric biosensor. The results revealed that the resulting biosensor exhibited very high affinity to its ligand, VEGF, and produced detectable response-based electrochemical impedance spectroscopy. The Kramers–Kronig transforms were applied to the biosensor system. These transforms showed that the impedance data obtained by the biosensor was stable, linear, and causal. Under optimal conditions the VEGF-R1 biosensor exhibited a linear range from 10 pg/mL to 70 pg/mL. The impedimetric biosensor also displayed excellent repeatability and reproducibility. In conclusion, the biosensor reported here could be a good alternative to other detection methods for VEGF in clinical analysis.

Acknowledgement

I gratefully acknowledge the financial support of TÜBİTAK (The Scientific and Technological Research Council of Turkey, Project number: 109T 172).

Appendix A. Supplementary data

Supplementary data associated with this article can be found, in the online version, at doi:10.1016/j.bios.2011.03.025.

References

Adams, J., Carder, P.J., Downey, S., Forbes, M.A., MacLennan, K., Allgar, V., Kaufman, S., Hallam, S., Bicknell, R., Walker, J.J., Cairnduff, F., Selby, P.J., Perren, T.J., Lansdown, M., Banks, R.E., 2000. Cancer Res. 60, 2898–2905.
Boffetta, P., 2010. J. Natl. Cancer Inst. 102, 142–143.
Bott, A.W., 2001. Curr. Sep. 19, 71–75.
Boukamp, B.A., 1995. J. Electrochem. Soc. 142, 1885–1894.
Conn, G., Soderman, D.D., Schaeffer, M.T., Wile, M., Hatcher, V.B., Thomas, K.A., 1990. Proc. Natl. Acad. Sci. USA 87 (4), 1323–1327.
Dhingra, K., Hortobagyi, G.N., 1996. Semin. Oncol. 23, 436–445.
Ding, S.J., Chang, b.W., Wu, C.C., Lai, M.R., Chang, H.C., 2005. Electrochim. Acta 50, 3660–3666.
Ehm, W., Gohr, H., Kaus, R., Roseler, B., Schiller, C.A., 2000. ACH Mod. Chem. 137, 145–157.
Gonzalez Campora, R., Galera Ruiz, M., Vazquez Ramirez, F., Rios Martin, J.J., Fernandez Santos, J.M., Martos, M.M., Gomez Pascual, A., 2000. Pathol. Res. Pract. 196, 167–174.
Guan, J.G., Miao, Y.Q., Zhang, Q.J., 2004. J. Biosci. Bioeng. 97, 219–226.
He, Y., Smith, S.K., Day, K.A., Clark, D.E., Licence, D.R., Charnock-Jones, D.S., 1999. Mol. Endocrin 13 (4), 537–545.
Huang, Q.A., Hui, R., Wang, B., Zhang, J., 2007. Electrochim. Acta 52, 8144–8164.
Katz, E., Willner, I., 2003. Electroanalysis 15, 913–947.
Kendall, R.L., Thomas, K.A., 1993. Proc. Natl. Acad. Sci. USA 90 (22), 10705–10709.
Kramers, H.A., 1929. Phys. Z. 30, 522–523.
Kronig, R.L., 1926. J. Opt. Soc. Am. Rev. Sci. Inst. 12, 547–557.
Kulasingam, V., Diamandis, E.P., 2007. Int. J. Cancer 123, 2007–2012.
Laguens, G., Coronato, S., Girolamo, W., 2010. Cent. Eur. J. Med. 1, 330–347.
Lee, H.S., Kim, K.S., Kim, C.J., Hahn, S.K., Jo, M.H., 2009. Biosens. Bioelectron. 24, 1801–1805.
Levenson, V.V., 2007. Biochim. Biophys. Acta 1770, 847–856.
Lo, H.W., Hsu, S.C., Hung, M.C., 2005. Breast Cancer Res. Treat. 28, 1–8.
Neufeld, G., Cohen, T., Gengrinovitch, S., Poltorak, Z., 1999. FASEB J 13 (1), 9–22.

Oldenburg, R.A., Meijers-Heijboer, H., Cornelisse, C.J., Devilee, P., 2007. Crit. Rev. Oncol. Hematol. 63, 125–149.
Olofsson, B., Korpelainen, E., Pepper, M.S., Mandriota, S.J., Aase, K., Kumar, V., Gunji, Y., Jeltsch, M.M., Shibuya, M., Alitalo, K., Eriksson, U., 1998. Proc. Natl. Acad. Sci. U.S.A. 95 (20), 11709–11714.
Orazem, M.E., Tribollet, B., 2008. Electrochemical Impedance Spectroscopy. John Wiley & Sons, New Jersey.
Pei, R., Cheng, Z., Wang, E., Yang, X., 2001. Biosens. Bioelectron. 16, 355–361.
Prabhulkar, S., Alwarappan, S., Liu, G., Li, C.-Z., 2009. Biosens. Bioelectron. 24, 3524–3530.
Qingwen, L., Hong, G., Yiming, W., Guoan, L., Jie, M., 2001. Electroanalysis 13, 1342–1346.
Rampaul, R.S., Pinder, S.E., Nicholson, R.I., Gullick, W.J., Robertson, J.F., Ellis, I.O., 2005. Adv. Anat. Pathol. 2005, 271–273.
Rochefort, H., Garcia, M., Glondu, M., Laurent, V., Liaudet, E., Rey, J., Roger, P., 2000. Clin. Chim. Acta 291, 157–170.
Sawyers, C.L., 2008. Nature 452, 548–552.
Shibuya, M., Yamaguchi, S., Yamane, A., Ikeda, T., Tojo, A., Matsushime, H., Sato, M., 1990. Oncogene 5, 519–524.
Sidoni, A., Cavalieri, G.A., D'Amico, G., Brachelente, G., Bucchiarelli, E., 2001. Breast 10, 325–329.
Sjostrom, J., Blomqvist, C., Heikkila, P., Bogulawski, K.V., Raiseanen-Sokolowski, A., Bengtsson, N.O., Majaaland, I., Malmstron, P., Ostenstadt, B., Berg, J., Wist, E., Valvere, V., Saksela, E., 2000. Clin. Cancer Res. 6, 3103–3110.
Wang, P., Whiteaker, J.R., Paulovich, A.G., 2009. Cancer Biol. Ther. 8, 1083–1094.